RESEARCH ARTICLE
doi: 10.2306/scienceasia1513-1874.2023.021

ScienceAsia 49 (2023): **344–352**

Dependence of applied electric fields on electrical properties of BCZT ceramic

Narongdetch Boothrawong[a,b], Lalita Tawee[b], Suwanan Thammarong[b], Pharatree Jaita[b,c,d], Dennis Russell Sweatman[b], Gobwute Rujijanagul[b,d,e,f,*], Tawee Tunkasiri[b,d]

[a] Graduate PhD's Degree Program in Applied Physics, Faculty of Science, Chiang Mai University, Chiang Mai 50200 Thailand
[b] Department of Physics and Materials Science, Faculty of Science, Chiang Mai University, Chiang Mai 50200 Thailand
[c] Office of Research Administration, Chiang Mai University, Chiang Mai 50200 Thailand
[d] Materials Science Research Center, Faculty of Science, Chiang Mai University, Chiang Mai 50200 Thailand
[e] Research Center in Physics and Astronomy, Faculty of Science, Chiang Mai University, Chiang Mai 50200 Thailand
[f] Science and Technology Research Institute, Chiang Mai University, Chiang Mai 50200 Thailand

*Corresponding author, e-mail: rujijanagul@yahoo.com

Received 5 Apr 2022, Accepted 3 Nov 2022
Available online 26 Feb 2023

ABSTRACT: It is vital to understand the characteristics of piezoelectric ceramics at high electric fields to use them effectively. The effects of applied electric fields such as applied electric and poling fields on the electrical characteristics of a (Ba,Ca)(Ti,Zr)O_3 or BCZT ceramic system were investigated in this research. A solid-state reaction process was used to make the BCZT ceramic. There was no impurity in the sample, which had a mixed phase of rhombohedral, tetragonal, and orthorhombic phases. A high degree of dielectric tunability was found under the applied electric fields. Large improvements in polarization prosperities were reported with non-linear relationships with the applied electric fields. The ferroelectric data matched with the electric field-induced strain behavior data, while the field-induced strain behavior data revealed a near-linear relationship with the field. There was also a significant reduction in the degree of strain hysteresis. In addition, the poling field had a significant impact on the d_{33} and g_{33} values. The piezoelectric coefficients discovered in this study suggest that this material has promise for use in piezoelectric and energy harvesting devices.

KEYWORDS: $BaTiO_3$-based, poling effect, piezoelectric ceramic, electrical properties

INTRODUCTION

Complex perovskite oxides are represented by $A(B'B'')O_3$ [1]. Because of their outstanding ferroelectric, piezoelectric, and dielectric capabilities, they are intensively investigated and developed. The perovskite oxide lead zirconate titanate, $Pb(Zr_xTi_{1-x})O_3$ (PZT), has remarkable electrical properties. Since the early 1950s, this material has been intensively researched [1]. The morphotropic phase boundary (MPB) of PZT is the border between tetragonal and rhombohedral phases (Zr/Ti∼53/47). At the phase transition temperature (T_C), at which the cubic phase occurs, the MPB boundary is practically temperature independent [1–3]. The best electrical characteristics of PZT were found in compositions around the MPB limit. Many piezoelectric materials have been devised and manufactured based on the MPB principle to achieve excellent characteristics [4–7] However, because of the toxicity of lead oxide, PZT and its modified materials are not ecologically benign. As a result, it is necessary to investigate lead-free piezoelectric ceramics with comparable qualities that might be utilized in place of lead-based ceramics such as PZT. Bismuth sodium titanate (BNT) and Barium zirconium titanate (BZT) are among the most researched lead-free ceramics [8–12]. Because of its good dielectric constant (with low loss) and ferroelectric and piezoelectric properties, this material looks like a good replacement for lead-based materials [10]. $BaTiO_3$ lattices can be substituted at the B-site with Zr ions to produce the BZT ceramic. The electrical and structural characteristics of $BaTiO_3$ are considerably altered by this replacement [13], A diffuse phase transition and relaxor ferroelectric behavior are among the features [8–10]. Zr concentration affects the transition temperatures of BZT from rhombohedral to orthorhombic (T_{R-O}), orthorhombic to tetragonal (T_{O-T}), and tetragonal to cubic (T_C) phases. Three phase transitions merge into a single diffuse transition when the Zr concentration is less than 15%. Zr concentrations of more than 25% have been observed with relaxor ferroelectric properties [8]. High dielectric tunability has also been reported for some compositions, especially for Zr ∼ 30 at% [10]. The modified BZT ceramics show many interesting electrical properties. For example, $Ba(Zr_{0.07}Ti_{0.93})O_3$ ceramics show good piezoelectric properties with high strain values [14]. Therefore, the BZT-based ceramics have the potential for multilayer capacitors, actuators, and sensors. Recently, the solid solution of BZT-based ceramics [15] demonstrated extremely high piezoelectric characteristics in comparison

to a number of well-known piezoelectric lead-based ceramics such as PZT and lead-free ceramics such as BZT-based ceramics [16]. The BZT-based materials, therefore, have potential for various device applications, including piezoelectric transducers and microelectromechanical systems (MEMS) [17]. Among BZT-based ceramics, BCZT ceramics also show good electrical properties. The BCZT-ceramics with the formula 0.5 $Ba(Zr_{0.2}Ti_{0.8})O_3$ - 0.5 $(Ba_{0.7}Ca_{0.3})TiO_3$ showed a high dielectric constant (3060), large k_p (0.50), and excellent piezoelectric response with a d_{33} of 500–600 pC/N [18, 19]. The high piezoelectric properties of BCZT were proposed to be due to the formation of multi-phase coexistence of R, O, and T phases that are closely linked to the morphotropic phase boundary (MPB) composition ($x = 0.5$) along with domain wall motion [20]. Furthermore, the piezoelectric properties of BCZT ceramics strongly depend on the ratio of Zr:Ti [3], grain size [21], porosity [3], method of preparation technique [3], and poling technique. Among them, the poling process is a method to promote the piezoelectric properties of many piezoelectric ceramics [15]. Normally, the electric poling can produce an alignment of domain, and the ceramics can be polarized with a non-zero polarization, which develops along the applied field direction [15, 22]. Furthermore, poling also impacts the coexistence of R, O, and T phases, reducing the energy barrier during polarization switching. This can improve the piezoelectric characteristics of several piezoelectric ceramics such as BCZT ceramics.

Therefore, it is crucial to evaluate the influence of the poling on the piezo-response of the studied ceramics. In the present work, the effect of poling conditions on the dielectric, ferroelectric, and piezoelectric properties of BCZT ceramic was investigated. The results were discussed and compared to what had been done previously.

MATERIALS AND METHODS

To prepare the $A(B'B'')O_3$ complex perovskite oxides, many methods have been demonstrated such as sol-gel [23], microwave-assisted sol-gel-hydrothermal [3], molten-salt [24], plasma-activated sintering [25], and solid-state reaction techniques. However, the solid-state reaction technique has attracted a lot of attention for the fabrication of BZT-based materials [26], due to it being cheaper and easier than many techniques. Furthermore, the yield product obtained from this technique is higher when compared with many other methods [27]. Reagent-grade oxide powders of $BaCO_3$, ZrO_2, $CaCO_3$, and TiO_2 from Sigma-Aldrich, St. Louis, MO, USA were used as raw materials. The metal oxide powders were weighed based on the stoichiometric formula of $(Ba_{0.85}Ca_{0.15})(Zr_{0.1}Ti_{0.9})O_3$(BCZT). The weighed batch was ball-milled in alcohol and zirconia milling media for 24 h in ethanol. The mixed

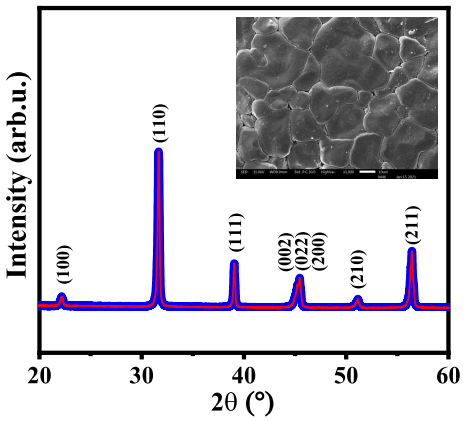

Fig. 1 XRD diffraction pattern of the BCZT sample. The inset figure shows a SEM image observed of the surface of sample.

powder was calcined at 1250 °C for 4 h. The obtained powders were pressed into disc-shape pellets 10 mm in diameter after adding with 4 wt % polyvinyl alcohol (Sigma-Aldrich) binder. After burnout PVA at 700 °C, the green pellets were sintered at 1450 °C for 4 h. Phase formation of the ceramics was studied by X-ray diffraction (Miniflex6g, Rigaku, Tokyo, Japan). The bulk density of the sintered samples was measured using the Archimedes method, ASTM C373-88. A microstructural study of the sintered samples was performed under a scanning electron microscope (JSM-IT300, JEOL, Tokyo, Japan). For the electrical study, a silver paste was painted on both sides of the samples. The hysteresis loops were measured at room temperature using a hysteresis circuit (Precision Premier II, Radiant technologies, Albuquerque, NM, USA). For piezoelectric measurement, the ceramics were placed in a silicone oil bath at room temperature for 30 min and with an electric field of 10–30 kV/cm, before the measurement. The piezoelectric coefficients d_{33} of the samples were measured using a d_{33} meter (S5865 d_{33} Meter, KCF technologies, State College, PA, USA). The planar electromechanical coupling coefficient k_p was tested by a resonance-antiresonance method using an impedance analyzer (E4980A, Agilent technologies, Santa Clara, CA, USA). Room temperature strain-electric field (S-E) data were obtained using an optical displacement sensor (MTI-2100 Fotonic sensor, MTI Instruments, Albany, NY, USA) combined with a Radiant ferroelectric test system.

RESULTS AND DISCUSSION

To study the phase formation, the obtained ceramics were examined by XRD at room temperature. Fig. 1 displays an XRD pattern of the obtained BCZT ceramic. The ceramic sample possessed a pure perovskite phase without minor peaks. Normally, the diffraction peaks of $BaTiO_3$ and BCZT at Bragg's angle around 44–46° correspond to (002)/(200)T of the tetragonal

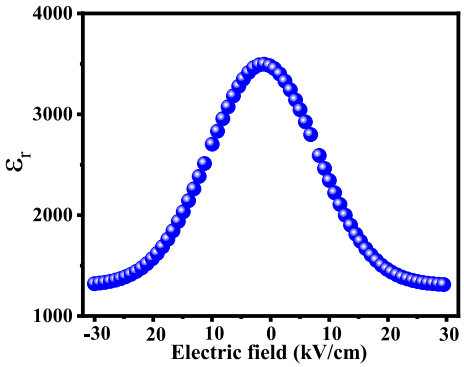

Fig. 2 Dielectric constant (ε_r) as a function of applied field of the studied BCZT sample.

phase (T), (200)R of the rhombohedral phase (R), and (200)/(220) of the orthorhombic phase (O) [28, 29]. Based on the XRD analysis, all the main diffraction peaks contained a mixed phase. The amounts of the T, R, and O phases were calculated by Jana 2006 software. In this work, percentage of T, R, and O phases as calculated from the software were 49, 31, and 20%, respectively.

SEM micrograph image of the sintered ceramic is shown in the inset of Fig. 1. From the SEM image, the ceramic shows clearly the crystalline boundaries with a round grain shape. The grain size of the sample was evaluated from SEM figures, assisted by ImageJ software. In this work, the average grain size was 16.6 µm. The obtained grain size value for this work is close to the value reported in previous work that sintered the samples at the same temperature [15]. This value is high as compared with the value obtained from $BaZr_{0.2}Ti_{0.8}O_3$(BZT) and BCZT ceramics. The sample also exhibited a dense, crack-free surface with few pores. This result consisted of the high-density value that was evaluated following ASTM C373-88, where the density in this work was 5.44 g/cm^3. The obtained density also agrees with values reported in many previous works [30]. This indicates that the sintering temperature in this work, 1450 °C for 4 h, is suitable for the fabrication of the ceramics (by using the solid-state reaction technique).

A plot of dielectric constant as a function of the applied field is displayed in Fig. 2. The measurement was conducted at room temperature. High tunability was observed for the studied sample. A sharp decrease in ε_r value was found for the applied field between 10–30 kV/cm, followed by a slight change for further applied fields. To check the degree of tunability of the dielectric constant, the relative tunability (n_r (%)) was calculated by the following expression [31].

$$n_r(\%) = \frac{\varepsilon_r(0) - \varepsilon_r(E)}{\varepsilon_r(0)} \times 100\% \qquad (1)$$

where $\varepsilon_r(0)$ and $\varepsilon_r(E)$ are the capacitance at zero and the higher electric field, respectively. In this work, the $\varepsilon_r(E)$ values were measured for the applied field 5 to 30 kV/cm. It was found that n_r of the sample was 62.3%. This value is very high as compared with other materials [32]. This indicates that this material has the potential for use in tunable device applications. The value was slightly changed in n_r value for the field $>$ 25 kV/cm, the tunable device should be operated under 30 kV/cm. For a near linear tunable device, it should be operated with the applied field between 5–15 kV/cm (Fig. 2).

Plots of polarization-electric field loops (P-E) as function applied electric field are shown in Fig. 3. For more detail, remanent polarization (P_r), maximum polarization (P_m), and coercive field (E_C) as a function of the applied electric field is also shown in Fig. 4 and Table 1. A non-linear relationship of P-E was observed for all conditions. No evidence of pinning effect or asymmetric loop was detected for all applied electric fields. At a low applied field such as 5 kV/cm, however, the P-E loop exhibited a weak ferroelectric ordering, which was evidenced by a slim with low P_r, P_m, and E_C values. However, in this field, the P-E loop still exhibited a ferroelectric characteristic. This indicates that this low electric field has enough energy to constrain the realignment of some domains in the direction of the applied fields [36], while this field could not switch any domains for some lead-based ceramics such as $Pb[(Zr_{1/2}Ti_{1/2})$-$(Zn_{1/3}Nb_{2/3})]O_3$ ceramic system, and results in the formation of a banana-like P-E loop at 5 kV/cm (or near-linear relationship of P-E) [36]. It was also found that the shape of hysteresis varies greatly with the electric field. Furthermore, the P_r and P_m values increased with increasing the applied field as depicted in Fig. 4(a) and Table 1. However, the increasing trends of P_r and P_m values with the applied field exhibited non-linear behavior. Instead, these values are consistent with some exponential functions. In this work, empirical relations between P_r and E_C values and the applied fields were developed, as expressed by $P_r = 14.14 - 13.72\exp(-0.066E)$ and $P_m = 23.19 - 23.72\exp(-0.093E)$, respectively. The E_C value versus the applied fields is presented in Fig. 4(b). It is interesting to note that E_C value increased with the applied field by a linear trend, which can be expressed as $E_C = 1.573 + 0.078E$.

Electric field-induced strain behavior of the ceramics obtained at room temperature and measured under various applied fields is presented in Fig. 5 and Table 1. The normalized strain coefficient (d^*_{33}) is also shown in Fig. 6. In this work, the d^*_{33} coefficient was calculated from the following equation [1, 37]:

$$d^*_{33} = \frac{S_{max}}{E_{max}}. \qquad (2)$$

The ceramic exhibited a typical butterfly-shaped strain

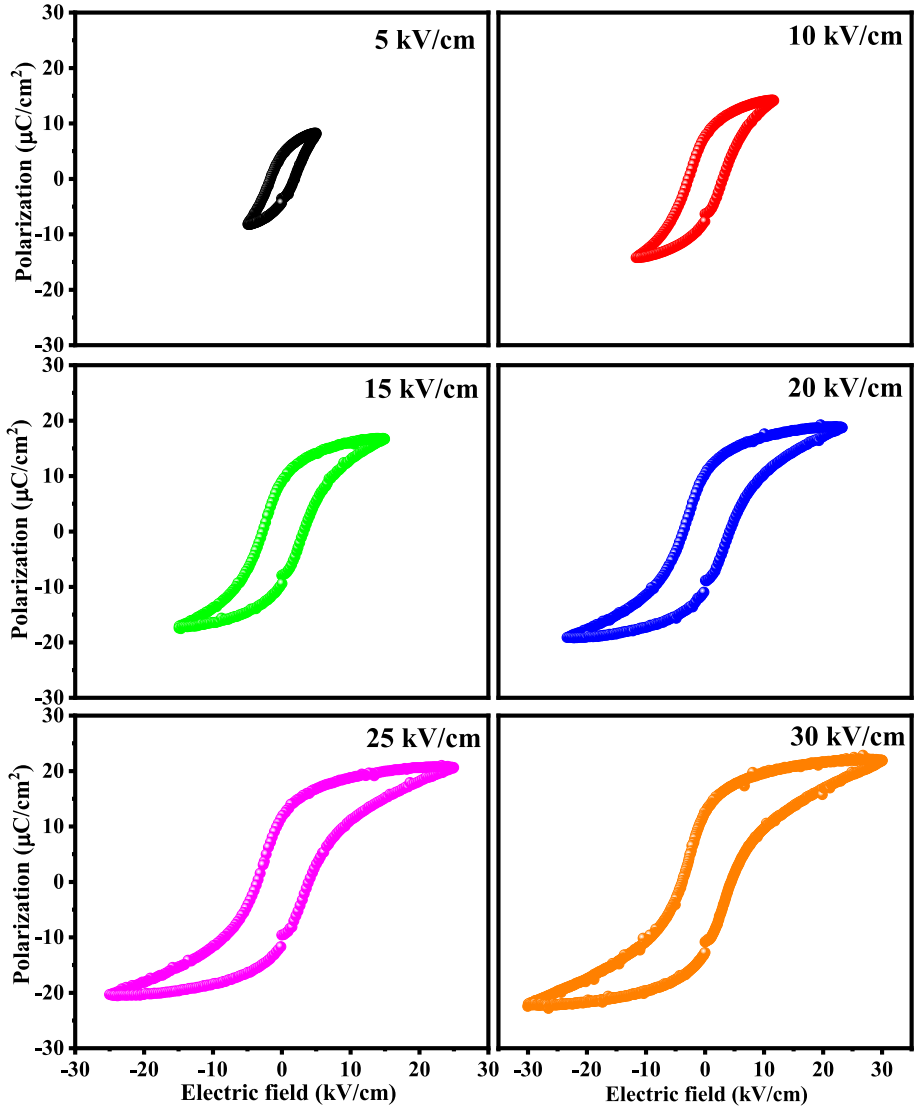

Fig. 3 Polarization-electric field loops (P-E) of the ceramics measured at room temperature and different applied electric fields.

Table 1 The summary of physical properties and electrical properties for BCZT-ceramic.

E_{poling} (kV/cm)	P_r (μC/cm^2)	P_m (μC/cm^2)	E_C (kV/cm)	S (%)	k_p	d^*_{33} (pm/V)	d_{33} (pC/N)	$g_{33} \times 10^{-3}$ (Vm/N)
10	7.53	14.14	2.40	0.056	0.39	560	364	15.88
20	10.60	19.94	3.12	0.117	0.54	585	485	33.56
30	12.42	21.83	3.88	0.151	0.55	503	490	42.14

loop corresponding with the P-E loop for all conditions. The S_{max} value has a nearly linear relation with the applied field which can be expressed as the equation: $S_{max} = 0.013 + 0.00475E$. However, the d^*_{33} coefficient has a non-linear relation with the applied field. The d^*_{33} coefficient was found to increase from 560 pm/V for the applied field of 10 kV/cm to 585 pm/V for the applied field of 20 kV/cm and then decreased to 503 pm/V for the applied field of 30 kV/cm (Table 1). Normally, the d^*_{33} coefficient can be calculated from the slope of the S-E loop, which has a non-linear behavior (see Fig. 5(c)). Therefore, the lower d^*_{33} coefficient can be caused by the increasing rate of S_{max} which is decreased by the high electric

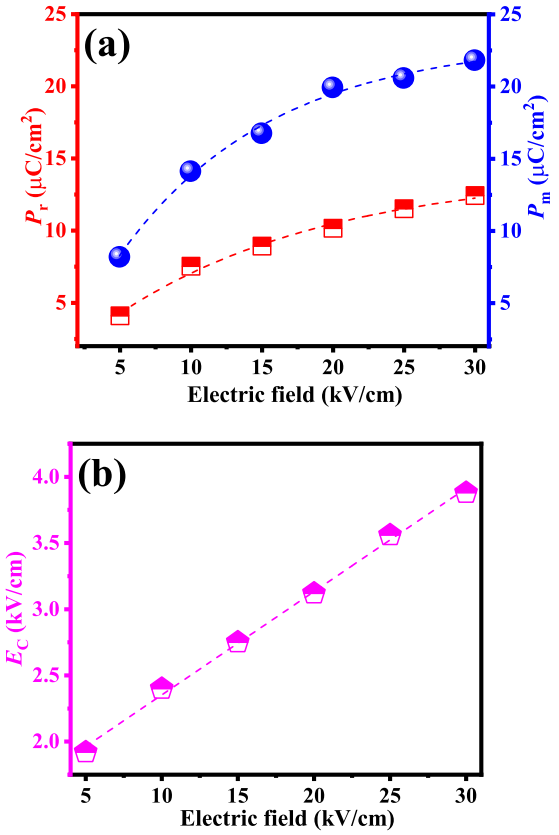

Fig. 4 (a) Plots of P_r and P_m versus applied field and (b) E_C value as a function of applied field.

fields. This is because the value of S_{max} is approaching its maximum value in the high field. Further increasing the field value may result in not only a small change in the increasing rate of S_{max} but also an electrical breakdown for the ceramics under consideration.

For piezoelectric actuator applications, high strain as well as low hysteresis are required. As a result, in this work, the degree of strain hysteresis (H_S (%)) was determined using the following equation [38]:

$$H_S = \frac{\Delta S_{Emax/2}}{S_{max}} \times 100\% \quad (3)$$

where the $\Delta S_{Emax/2}$ is the strain deviation during the removal and application of the field which is carried out at half of the maximum electric field. The H_S values versus the applied field of the ceramics are given in Fig. 6. The trend of H_S value with the applied field is nearly linear, where the H_S value obviously decreased from 70.71% for the applied field of 10 kV/cm to 14.57% for the applied field of 30 kV/cm. The change of H_S value under the change the in applied field was 79.39%. This result clearly demonstrates that the hysteresis in the ceramic can be obviously reduced by the applied field. In the present work, the linear

Table 2 Comparison of the piezoelectric properties of BCZT-ceramic with other works.

Composition	d_{33} (pC/N)	Ref.
$(Bi_{1/2}Na_{1/2})TiO_3$	66	[33]
$BaTiO_3$	190	[34]
$BiFeO_3$	402	[34]
$(K_{1/2}Na_{1/2})NbO_3$	416	[35]
$(Ba_{0.85}Ca_{0.15})(Zr_{0.1}Ti_{0.9})O_3$	490	This work

relation between H_S value and the applied field is expressed as $H_S = 95.11 - 2.807E$.

For some applications of piezoelectric devices, it is necessary to have a highly efficient energy conversion [39]. Normally, energy transfer is often considered when the device is operated at piezo-mechanical resonant frequencies [40]. At the resonance state, the piezoelectric devices efficiently convert electrical energy into mechanical energy. Therefore, it is needed to know these frequencies for applications. An effective way to measure these frequencies is by using impedance spectroscopy. This can be performed by using an impedance versus frequency plot (Z-f). To achieve this, the ceramic was poled at various poling fields. Fig. 7(a-c) displays the impedance value versus frequency for different poling fields. There were two resonance frequencies in the Z-f plots which indicated the resonance state. Based on the obtained Z-f plots, the electromechanical coupling coefficient (k_p) was calculated via the following equation [41].

$$k_p = \left(\frac{2.51(f_a - f_r)}{f_a}\right)^{1/2} \quad (4)$$

where f_r and f_a are the resonance and anti-resonance frequencies, respectively. This parameter can measure the degree of energy conversion. The k_p value sharp increased from 38.55% for the poling field of 10 kV/cm to 54.31% for the poling field of 20 kV/cm and slightly increased to 55.16% for the poling field of 30 kV/cm (Table 1). The maximum k_p value for this work is comparably high as compared with many lead-based and lead-free materials [23]. Overall obtained results indicated that poling field had a strong effect on the k_p value. It should be noted that, at a low poling field, the k_p was very low. This is due to the low poling field making the polarization switching inadequate [42]. However, this effect has a limit, since the k_p for the high poling field (30 kV/cm) was only slightly changed as compared with that obtained for the field of 20 kV/cm. Furthermore, a high poling field (> 30 kV/cm) may lead to the dielectric breakdown of the studied sample due to the formation of physical flaws and conduction paths during the poling [15, 43].

To study the piezoelectric properties of the sample, a piezoelectric coefficient (d_{33}) under different electrical poling fields was evaluated. The results are

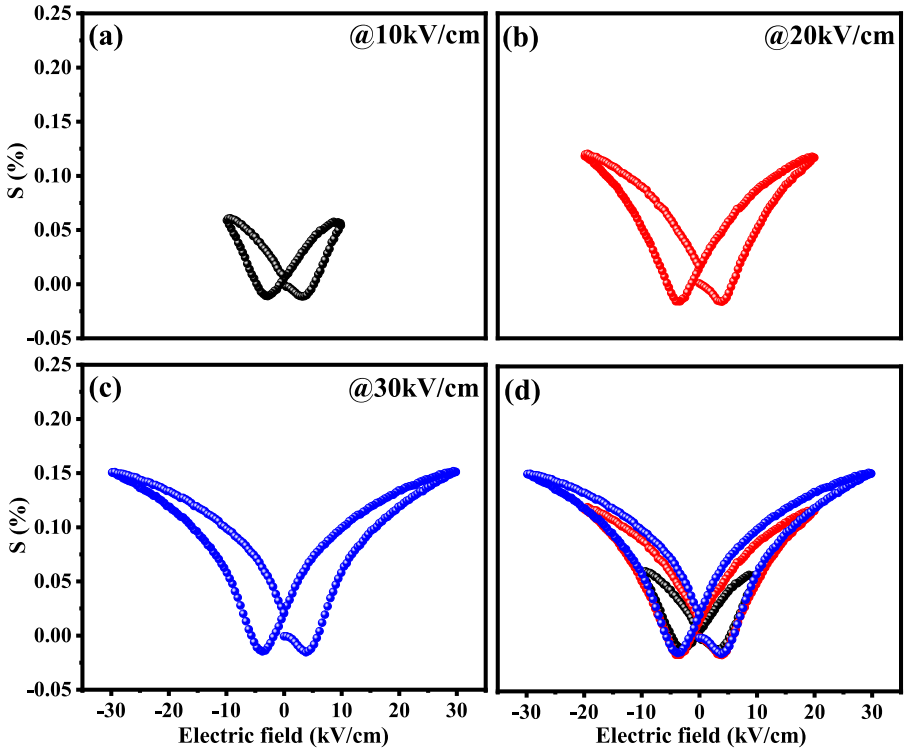

Fig. 5 Electric field-induced strain behavior of the BCZT ceramics at various applied electric fields.

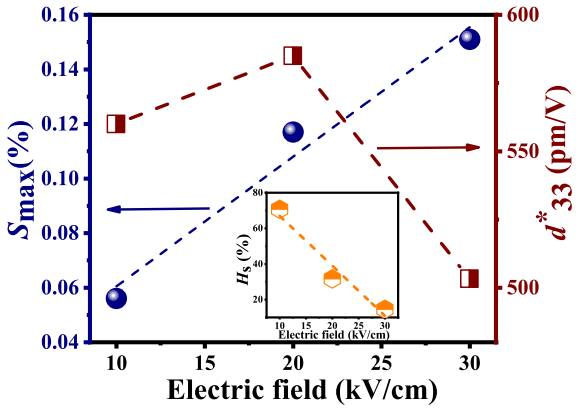

Fig. 6 Plot of maximum strain (S_{max}) values and normalized strain coefficient ($d^*_{33} = S_{max}/E_{max}$) as a function of electric field. The inset shows H_s values versus the applied field of the ceramics.

presented in Fig. 8. In this work, the d_{33} value was determined from the d_{33} meter as described in the experimental part. At the poling field of 10 kV/cm, the sample showed a d_{33} value of 364 pC/N. There was a sharp increase in the d_{33} value from this value to 485 pC/N (for the poling field of 20 kV/cm), followed by a slight increase of this value for the poling field of 30 kV/cm. The maximum d_{33} value (at 30 kV/cm) was 490 pC/N which is a 34% improvement as compared with the sample at 10 kV/cm. This maximum value is considered high as compared with many previous works [44]. The high d_{33} value in this work is due to the formation of mixture phases (multi-ferroelectric phase) in the sample after sintering (described in the previous part), as it is known that the optimization of the multiphase coexistence can enhance the electrical properties of BCZT ceramics [44]. A comparison of d_{33} value between this work and other works is shown in Table 2 [33–35]. It should be noted that the present samples had high d_{33} value as compared with other systems.

At present, piezoelectric materials are attractive for the development of energy harvesting applications. In this work, energy harvesting properties of the studied ceramics were carried out. It is known that the piezoelectric voltage constant (g_{33}) is an important factor for an energy harvester. Normally, a material that has a higher g_{33} value can generate a higher voltage output under given conditions [45, 46]. This parameter can be an indicator of evaluating the amount of electrical energy generated by the applied pressure [47, 48]. Furthermore, it was suggested that the sample which has a higher piezoelectric charge constant should generate a higher voltage [47]. A plot the of g_{33} value as a function of poling field is also shown in Fig. 8(a). In this work, the g_{33} value was calculated using the following equation [48], as seen

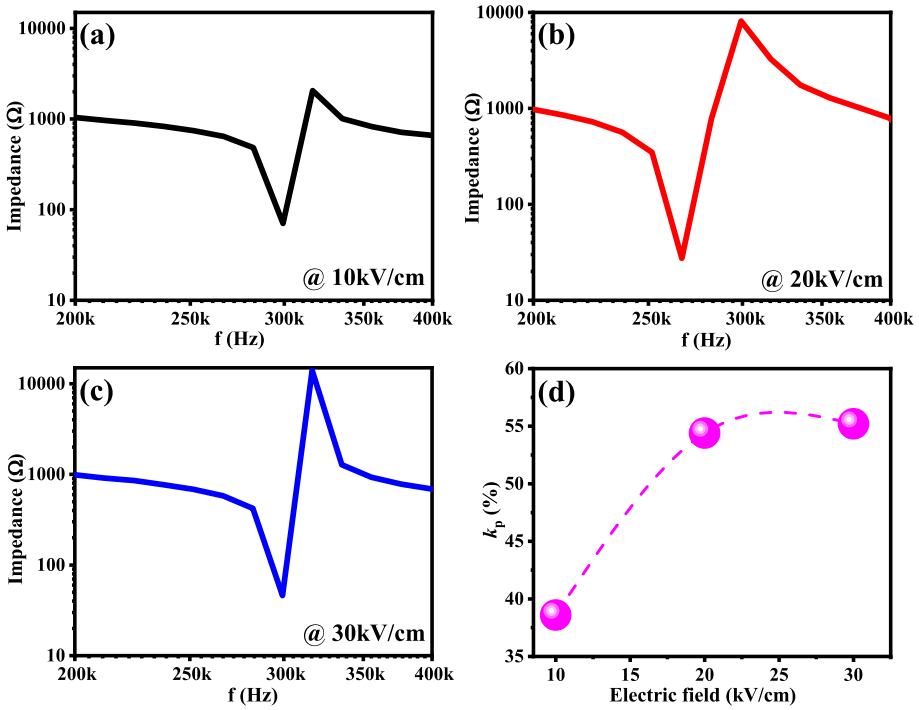

Fig. 7 (a-c) Impedance versus frequency for various poling electric fields and (d) with respect for the poled BCZT samples.

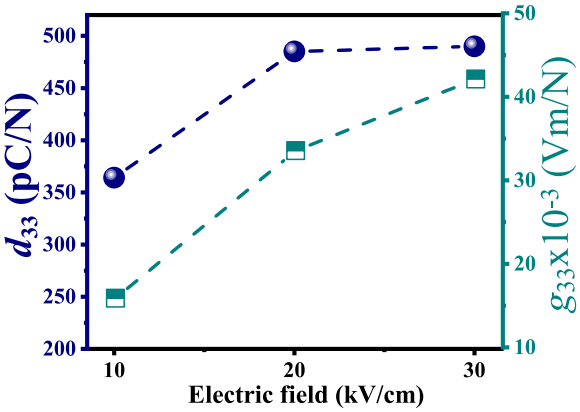

Fig. 8 Piezoelectric coefficient (d_{33}) and piezoelectric voltage coefficient (g_{33}) as a function of poling field.

in Table 1.

$$g_{33} = \frac{d_{33}}{\varepsilon_o \varepsilon_r} \tag{5}$$

where ε_o is the permittivity of free space and ε_r is the dielectric constant. For this equation, the piezoelectric voltage coefficient is dependent on the piezoelectric coefficient and the dielectric constant of the studied material. The g_{33} value increased with the poling field and showed the maximum value of 42.2×10^{-3} Vm/N at the poling field of 30 kV/cm, which is 165% enhanced as compared with the sample at 10 kV/cm poling (15.9×10^{-3} Vm/N). The increasing trend in the g_{33} value is due to the increase in the d_{33} value. The obtained result also indicates that the poling field has a very strong effect on the g_{33} value. Furthermore, the obtained piezoelectric coefficient suggested a potential for using this material for piezoelectric and energy harvesting devices.

CONCLUSION

A dense with no impurity BCZT ceramic was successfully fabricated via a solid-state reaction technique at 1450 °C for 4 h. The ceramic contained the mixture phases of rhombohedral, tetragonal, and orthorhombic phases with a large grain size of 16.6 µm. Effects of applied electric field on the electrical properties were investigated. A high degree of dielectric tunability of 62.3% was observed at 25 kV/cm. Polarization properties exhibited non-linear behaviors with the applied field, while electric strain possessed a near linear behavior. A large change in the degree of hysteresis of the strain loop was also observed (79.39%). The d_{33} and g_{33} piezoelectric coefficients also had a large effect on the poling field. This material has the potential for use in piezoelectric and energy harvesting devices.

Acknowledgements: This research work is funded by National Research Council of Thailand (NRCT5-RSA63004, NRCT5-RSA63004-03) and partially supported by Chiang Mai University, Science Achievement Scholarship of Thailand (SAST), Materials Science Research Center, Global Partnership Project (B16F640001), Research Center in Physics and

Astronomy. Graduate School, Office of Research Administration, Department of Physics and Materials Science, Faculty of Science, and Science and Technology Research Institute, Chiang Mai University are also acknowledged.

REFERENCES

1. Moulson AJ, Herbert JM (2003) *Electroceramics: Materials, Properties, Applications*, John Wiley & Sons. New York, USA.
2. Charoenthai N, Traiphol R, Rujijanagul G (2008) Microwave synthesis of barium iron niobate and dielectric properties. *Mater Lett* **62**, 4446–4448.
3. Vittayakorn N, Uttiya S, Rujijanagul G, Cann DP (2005) Dielectric and ferroelectric characteristics of 0.7PZT-0.3PZN ceramics substituted with Sr. *J Phys D Appl Phys* **38**, 2942–2946.
4. Choi S, Shrout RT, Jang S, Bhalla A (1989) Dielectric and pyroelectric properties in the $Pb(Mg_{1/3}Nb_{2/3})O_3$-$PbTiO_3$ system. *Ferroelectrics* **100**, 29–38.
5. Praveen JP, Karthik T, James A, Chandrakala E, Asthana S, Das D (2015) Effect of poling process on piezoelectric properties of sol-gel derived BZT-BCT ceramics. *J Eur Ceram Soc* **35**, 1785–1798.
6. Rujijanagul G, Boonyakul S, Tunkasiri T (2001) Effect of the particle size of PZT on the microstructure and the piezoelectric properties of 0-3 PZT/polymer composites. *J Mater Sci Lett* **20**, 1943–1945.
7. Chaipanich A, Rujijanagul G, Tunkasiri T (2009) Properties of Sr- and Sb-doped PZT-Portland cement composites. *Appl Phys A* **94**, 329–337.
8. Zhi Y, Guo R, Bhalla A (2000) Dielectric behavior of $Ba(Ti_{1-x}Zr_x)O_3$ single crystals. *J Appl Phys* **88**, 410–415.
9. Bhaskar RS, Prasad RK, Rao R (2007) Structural and dielectric characterization of Sr substituted $Ba(Zr,Ti)O_3$ based functional materials. *Appl Phys A* **89**, 1011–1015.
10. Yu Z, Ang C, Guo R, Bhalla A (2002) Dielectric properties and high tunability of $Ba(Ti_{0.7}Zr_{0.3})O_3$ ceramics under dc electric field. *Appl Phys Lett* **81**, 1285–1287.
11. Jaita P, Sanjoom R, Lertcumfu N, Malasri P, Rujijangul G, Tunkasiri T (2020) Effect of barium iron tantalate incorporation on mechanical, electrical, and magnetocapacitance properties of modified bismuth sodium potassium titanate ceramics. *ScienceAsia* **46S**, 66–73.
12. Saenkam K, Jaita P, Sirisoonthorn S, Tunkasiri T, Rujijangul G (2021) Effects of processing parameter on energy storage density and ferroelectric properties of lead-free bismuth sodium titanate-strontium bismuth titanate ceramics. *ScienceAsia* **47S**, 34–41.
13. Ciomaga C, Buscaglia M, Viviani M, Buscaglia V, Mitoseriu L, Stancu A, Nanni P (2006) Preparation and dielectric properties of $BaZr_{0.1}Ti_{0.9}O_3$ ceramics with different grain sizes. *Ph Transit* **79**, 389–397.
14. Jarupoom P, Rujijanagul G (2013) Improvement in piezoelectric strain of annealed $Ba(Zr_{0.07}Ti_{0.93})O_3$ based ceramics. *J Appl Phys* **114**, 027018–027021.
15. Su S, Zuo R, Lu S, Xu Z, Wang X, Li L (2011) Poling dependence and stability of piezoelectric properties of $Ba(Zr_{0.2}Ti_{0.8})O_3$-$(Ba_{0.7}Ca_{0.3})TiO_3$ ceramics with huge piezoelectric coefficients. *Curr Appl Phys* **11**, S120–S123.
16. Jarupoom P, Pengpat K, Rujijanagul G (2010) Enhanced piezoelectric properties and lowered sintering temperature of $Ba(Zr_{0.07}Ti_{0.93})O_3$ by B_2O_3 addition. *Curr Appl Phys* **10**, 557–560.
17. Li F, Jin L, Guo R (2014) High electrostrictive coefficient Q_{33} in lead-free $Ba(Zr_{0.2}Ti_{0.8})O_3$-$x(Ba_{0.7}Ca_{0.3})TiO_3$ piezoelectric ceramics. *Appl Phys Lett* **105**, 232903–232906.
18. Swain AB, Kumar SD, Subramanian V, Murugavel P (2019) Influence of external electric field on the physical characteristics of lead-free BZT-BCT piezoceramic. *J Alloys Compd* **787**, 990–995.
19. Liu W, Ren X (2009) Large piezoelectric effect in Pb-free ceramics. *Phys Rev Lett* **103**, 257602–257605.
20. Gao J, Hu X, Zhang L, Li F, Zhang L, Wang Y, Hao Y, Zhong L, Ren X (2014) Major contributor to the large piezoelectric response in $(1-x)Ba(Zr_{0.2}Ti_{0.8})O_3$-$x(Ba_{0.7}Ca_{0.3})TiO_3$ ceramics: domain wall motion. *Appl Phys Lett* **104**, 252909–252913.
21. Bijalwan V, Tofel P, Holcman V (2018) Grain size dependence of the microstructures and functional properties of $(Ba_{0.85}Ca_{0.15-x}Ce_x)(Zr_{0.1}Ti_{0.9})O_3$ lead-free piezoelectric ceramics. *J Asian Ceram Soc* **6**, 384–393.
22. Li B, Ehmk MC, Blendell JE, Bowman KJ (2013) Optimizing electrical poling for tetragonal, lead-free BZT-BCT piezoceramic alloys. *J Eur Ceram Soc* **33**, 3037–3044.
23. James AR, Kumar A (2019) Development of PLZT electroceramics with ultrahigh piezoelectric properties by a novel material engineering approach. In: *Handbook of Advanced Ceramics and Composites*, Springer, Switzerland, pp 215–250.
24. Tawichai N, Sittiyot W, Eitssayeam S, Pengpat K, Tunkasiri T, Rujijanagul G (2012) Preparation and dielectric properties of barium iron niobate by molten-salt synthesis. *Ceram Int* **38**, S121–S124.
25. Li S, Wang C, Ji X, Shen Q, Zhang L (2017) Effect of composition fluctuation on structural and electrical properties of BZT-xBCT ceramics prepared by plasma activated sintering. *J Eur Ceram Soc* **37**, 2067–2072.
26. Maraj M, Wei W, Peng B, Sun W (2019) Dielectric and energy storage properties of $Ba_{(1-x)}Ca_xZr_yTi_{(1-y)}O_3$ (BCZT): a review. *Mater* **12**, 3641–3666.
27. Eitssayeam S, Intatha U, Pengpat K, Rujijanagul G, MacKenzie K, Tunkasiri T (2009) Effect of the solid-state synthesis parameters on the physical and electronic properties of perovskite-type $Ba(FeNb)_{0.5}O_3$ ceramics. *Curr Appl Phys* **9**, 993–996.
28. Zhang Q, Cai W, Li Q, Gao R, Chen G, Deng X, Wang Z, Cao X, Fu C (2019) Enhanced piezoelectric response of $(Ba,Ca)(Ti,Zr)O_3$ ceramics by super large grain size and construction of phase boundary. *J Alloys Compd* **794**, 542–552.
29. Coondoo I, Panwar N, Alikin D, Bdikin I, Islam SS, Turygin A, Shur VY, Kholkin AL (2018) A comparative study of structural and electrical properties in lead-free BCZT ceramics: influence of the synthesis method. *Acta Mater* **155**, 331–342.
30. Bai Y, Matousek A, Tofel P, Bijalwan V, Nan B, Hughes H, Button TW (2015) $(Ba,Ca)(Zr,Ti)O_3$ lead-free piezoelectric ceramics the critical role of processing on properties. *J Eur Ceram Soc* **35**, 3445–3456.
31. Syal R, Kumar M, Singh AK, De A, Thakur O, Kumar S (2020) Enhancement in the piezoelectric properties in lead-free BZT-xBCT dense ceramics. *J Mater Sci Mater*

Electron **31**, 21651–21660.
32. Wei X, Feng Y, Hang L, Yao X (2004) Dielectric properties of barium stannate titanate ceramics under bias field. *Ceram Int* **30**, 1401–1404.
33. Wang X, Chan LW, Choy CL (2003) $(Bi_{1/2}Na_{1/2})TiO_3$-$Ba(Cu_{1/2}W_{1/2})O_3$ Lead-free piezoelectric ceramics. *J Am Ceram Soc* **86**, 1809–1811.
34. Lee MH, Kim DJ, Park JS, Kim SW, Song TK, Kim MH, Kim WJ, Do D, Jeong IK (2015) High-performance lead-free piezoceramics with high curie temperatures. *Adv Mater* **27**, 6976–6982.
35. Zhang B, Wu J, Cheng X, Wang X, Xiao D, Zhu J, Wang X, Lou X (2013) Lead-free piezoelectrics based on potassium-sodium niobate with giant d_{33}. *ACS Appl Mater Interfaces* **5**, 7718–7725.
36. Kruea-In C, Eitssayeam S, Pengpat K, Tunkasirit T, Rujijanagul G (2011) Effect of vibro-milling on dielectric properties of barium zirconium titanate ceramics. *Ferroelectrics* **415**, 135–140.
37. Vittayakorn N, Rujijanagul G, Cann DP (2007) The improvement in dielectric and ferroelectric performance of PZT-PZN ceramics by thermal treatment. *Curr Appl Phys* **7**, 582–585.
38. Xie H, Zhao Y, Xu J, Yang L, Zhou C, Zhang H, Zhang X, Qiu W, Wang H (2018) Structure, dielectric, ferroelectric, and field-induced strain response properties of $(Mg_{1/3}Nb_{2/3})^{4+}$ complex-ion modified $Bi_{0.5}(Na_{0.82}K_{0.18})_{0.5}TiO_3$ lead-free ceramics. *J Alloys Compd* **743**, 73–82.
39. Jarupoom P, Jaita P, Sweatman DR, Watcharapasorn A, Rujijanagul G (2022) Enhancement of electrostrictive and magnetic performance with high energy storage efficiency in Fe_2O_3 nanoparticles-modified $Ba(Zr_{0.07}Ti_{0.93})O_3$ multiferroic ceramics. *Mater Sci Eng B* **277**, 115579–115590.
40. Chavan D, Naik LR (2016) Structural and magnetic properties of $NiFe_2O_4$+$BaZr_{0.2}Ti_{0.8}O_3$ ME composites for sensor applications. *J Adv Sci Tecnol* **12**, 330–333.
41. Swain AB, Kumar SD, Subramanian V, Murugavel P (2019) Influence of external electric field on the physical characteristics of lead-free BZT-BCT piezoceramic. *J Alloys Compd* **787**, 990–995.
42. Praveen JP, Karthik T, James AR, Chandrakala E, Asthana S, Das D (2015) Effect of poling process on piezoelectric properties of sol-gel derived BZT-BCT ceramics. *J Eur Ceram Soc* **35**, 1785–1798.
43. Tunkasiri T, Rujijanagul G (1996) Dielectric strength of fine-grained barium titanate ceramics. *J Mater Sci Lett* **15**, 1767–1769.
44. Yang Y, Zhou Y, Ren J, Zheng Q, Lam KH, Lin D (2018) Phase coexistence and large piezoelectricity in $BaTiO_3$-$CaSnO_3$ lead-free ceramics. *J Am Ceram Soc* **101**, 2594–2605.
45. Pengpat K, Jarupoom P, Kantha P, Eitssayeam S, Intatha U, Rujijanagul G, Tunkasiri T (2008) Phase formation and electrical properties of lead-free bismuth sodium titanate-potassium niobate ceramics. *Curr Appl Phys* **8**, 241–245.
46. Huang Y, Zhao C, Lv X, Wang H, Wu J (2017) Multiphase coexistence and enhanced electrical properties in $(1-x-y)BaTiO_3$-$xCaTiO_3$-$yBaZrO_3$ lead-free ceramics. *Ceram Int* **43**, 13516–13523.
47. Manotham S, Jaita P, Butnoi P, Lertcumfu N, Rujijanagul G (2022) Improvements of depolarization temperature, piezoelectric and energy harvesting properties of BNT-based ceramics by doping an interstitial dopant. *J Alloys Compd* **897**, 163021–163032.
48. Bammannavar B, Chavan G, Naik LR, Chougule B (2009) Magnetic properties and magnetoelectric (ME) effect in ferroelectric rich $Ni_{0.2}Co_{0.8}Fe_2O_4$ + $PbZr_{0.8}Ti_{0.2}O_3$ ME composites. *Mater Chem Phys* **117**, 46–50.